



Published on behalf of the Latin American Association of Paleomagnetism and Geomagnetism by the Instituto de Geofísica, Universidad Nacional Autónoma de México.

**A preliminary rock magnetic
characterization of Fe-oxides
synthesized by co-precipitation of Fe
Ions in *Aloe vera***

V. Costanzo-Álvarez, P. Kryczka, J. Guerra, M. Aldana,
D. Bolívar, J.C. Guzmán.

18 pages, 7 figures, 1 table

Latinmag Letters can be viewed and copied free of charge at:
<http://www.geofisica.unam.mx/LatinmagLetters/>

Papers contents can be reproduced meanwhile the source is cited



A preliminary rock magnetic characterization of Fe-oxides synthesized by co-precipitation of Fe ions in *Aloe vera*

Vincenzo Costanzo-Álvarez^{1*}, Przemyslaw Kryczka², Julia Guerra³, Milagrosa Aldana¹, Diana Bolívar⁴, Juan Carlos Guzmán⁴

¹ Dpto. de Ciencias de la Tierra, Universidad Simón Bolívar, Caracas, Venezuela,

² Mag-Instruments UG Schellingstr. 109a, 80798 Munchen, Germany, kryczka@mag-instruments.com

³ Departamento de Termodinámica y Fenómenos de Transferencia, Universidad Simón Bolívar, Caracas, Venezuela, jguerra@usb.ve

⁴ Coordinación de Ingeniería Química, Universidad Simón Bolívar, Caracas, Venezuela

* corresponding e-mail: vcosta@usb.ve

Received: 23 August 2017; Accepted: 10 November 2017; Published: 22 Noviembre 2017

Abstract. This work presents a preliminary rock magnetic characterization of four Fe-oxides samples (MDaloe, MDpectin, P1 and P2 samples). The study was performed in order to know the nature, oxidation state, particle sizes and approximate shapes of these oxides, synthesized at room temperature via co-precipitation of Fe salts in pectin from *Aloe vera*. All the rock magnetic measurements were carried out in a versatile, highly sensitive (5×10^{-6} Am²/kg) and unique Variable Field Translation Balance (VFTB). The analysis of the thermomagnetic (high and low temperatures), thermosusceptibility and isothermal remanent magnetization (IRM) curves, reveal the presence of magnetite, largely oxidized to maghemite. Hysteresis parameters for MDaloe and MDpectin samples indicate that they contain non-stoichiometric multidomain (MD) magnetite. On the other hand, P1 and P2 samples seem to have maghemitized fine-grained magnetites of about 10 nm of diameter (superparamagnetic / single domain threshold), with cubic (P1) and acicular (P2) shapes. The mmol total Fe/meq COO ratios in the biomass (pectin), used in the synthesis of these samples, might have conditioned the growth, ordering and geometry of the magnetite particles.

Key words: Aloe Vera, green synthesis, maghemite, nanomagnetites, superparamagnetism, variable translation field balance

RESUMEN. Este trabajo presenta una caracterización magnética preliminar de cuatro muestras de óxidos de Fe (muestras MDaloe, MDpectin, P1 y P2). Este estudio se llevó a cabo para conocer la naturaleza, estado de oxidación, tamaños y formas aproximadas de dichos óxidos, sintetizados a temperatura ambiente a través de la co-precipitación de sales de Fe en pectinas de *Aloe vera*. Todas las mediciones magnéticas se hicieron en una balanza única de translación de campo variable (VFTB por sus siglas en inglés), particularmente versátil y altamente sensible (5×10^{-6} Am²/kg). El análisis de las curvas termomagnéticas (altas y bajas temperaturas), termosusceptibilidad y magnetización remanente isoterma (IRM) revelan la presencia de magnetita altamente oxidada a maghemita. Los parámetros de histéresis para las muestras MDaloe y MDpectin indican que contienen magnetita no estioquiométrica de dominio múltiple (MD). Por otro lado, las muestras P1 y P2 parecen tener magnetitas maghemitizadas de aproximadamente 10 nm de diámetro (límite superparamagnético/dominio simple) con formas de cubos (P1) y de agujas (P2). Las proporciones totales de FeO/meq COO en la biomasa (pectina), utilizadas en la síntesis de estas muestras, podrían haber condicionado el crecimiento, el orden y la geometría de las partículas de magnetita

Palabras clave: Aloe Vera, síntesis verde, maghemita, nanomagnetitas, superparamagnetismo, balanza de translación de campo variable.

1. Introduction

Synthetic magnetites (Fe₃O₄) have magnetic properties linked to their size and shape distributions. These granulometric parameters are in turn, associated to the multiple applications of this mineral in the micro (*i.e.* ca 10⁻⁶ m) and the nano (*i.e.* ca 10⁻⁹ m) diameter ranges. Nanomagnetites, below a size threshold



between 20 to 30 nm, might exhibit superparamagnetic (SP) behavior at room temperature. Above such a limit (*i.e.* between 30 and 80 nm) they become stable single-domain (SD), and over 80 – 100 nm, they will internally divide themselves into multiple magnetic domains (MD), to reduce their magnetostatic energy. There is a large variety of applications of nanomagnetites in biotechnology and medicine (*e.g.* Pankhurst, 2003; Lao and Ramanujan, 2004; Gupta and Gupta 2005; Mornet *et al.* 2006; Ramanujan and Lao 2006; Lu *et al.* 2007; Lang *et al.*, 2007; Shubayev *et al.*, 2009; Kim *et al.*, 2009; Sensenig *et al.*, 2012; Mendoza *et al.*, 2013; Priya James *et al.*, 2014; Kenawy *et al.*, 2014), in ferrofluids (*e.g.* Kaiser and Miskolczy 1970; Chikazumi *et al.*, 1987; Zahn, 2001), in magnetic recording media and data storage (*e.g.* Kang *et al.* 1996; Hyeon, 2003) and in natural waters remediation (*e.g.* Elliott and Zhang 2001; Shipley *et al.*, 2009; Chowdhury *et al.*, 2010; Zhao *et al.*, 2011; Chowdhury and Yanful 2013; Giraldo *et al.*, 2013; Liu *et al.*, 2015). The methods used for the synthesis of these particles have been thoroughly documented in the literature. Some of them include low temperature thermochemical precipitation reactions in solutions, namely co-precipitation from iron salts (*e.g.* Massart 1981; Visalakshi *et al.*, 1993; Kang *et al.*, 1996; Qu *et al.*, 1999; Sahoo *et al.* 2001; Tang *et al.*, 2003) and microemulsion (*e.g.* Chhabra *et al.*, 1996; Deng *et al.* 1999). Some other techniques, involve high temperatures processes (*e.g.* Gonzalez-Catteno *et al.*, 1993, Daichuan *et al.*, 1995, Li *et al.*, 1998, Worm and Markert 1987). The controlled chemical co-precipitation method is widely used due to its simplicity. However, it has not been until quite recently, when attempts to produce magnetite nanoparticles at low temperatures, using aqueous solutions, have proven successful (*e.g.* Nyiro-Kosa *et al.*, 2009; Perez-Gonzalez *et al.*, 2011). An alternative way to conventional co-precipitation methods is the so-called *Green Synthesis* which involves organisms such as bacteria, fungi and plants, as directing or guiding agents in the formation of the magnetic phases (Bharde *et al.*, 2005 and 2006; Philip 2009; Cai *et al.*, 2010; Foba-Tendo *et al.*, 2013 among others).

This study presents a preliminary rock magnetic characterization of Fe-oxides: MDaloe, MDpectin, P1 and P2, that are the by-product of a first attempt to green-synthesize, at room temperature, microscopic magnetites via co-precipitation of Fe-ions in *Aloe vera* and a commercial pectin also derived from *Aloe vera* (MDpectin). Non-magnetic analyses, carried out on these synthetic Fe-oxides, namely Energy-dispersive X-ray spectroscopy (EDX) and X-ray diffraction (XRD), in scanning electronic microscopy (SEM) and transmission electronic microscopy (TEM) respectively, turned out to be inconclusive about their nature and characteristics. This fact is even more crucial in the case of magnetically weakest P1 and P2, obtained from an unsaturated solution of Fe-salts, after several trials seeking for a decrease of the resulting particle sizes. Moreover, due to their high surface area/volume ratio, microscopic Fe-oxides are intrinsically unstable, tending to cluster and to be readily oxidized in the presence of oxygen. Thus, the rock magnetic experiments carried out on these samples, are aimed at testing the quality of these alleged magnetite particles by unraveling their nature and oxidation state (*i.e.* thermosusceptibility, thermomagnetic and isothermal remanent magnetization IRM curves) as well as their granulometric characteristics (*i.e.* hysteresis parameters).

The present work is the initial step of a joint venture, between the Departments of Thermodynamics and Transfer Phenomena and Earth Sciences (Universidad Simón Bolívar, Caracas), in collaboration with



Mag-Instruments UG (Munich), to develop a controlled production of microscopic magnetites, with particular magnetic properties, for environmental remediation purposes.

2. Samples

Fe-oxides in MDaloe, MDpectin, P1 and P2 samples were synthesized in a solution of magnetite precursors: ferric chloride and ferrous sulfate hexahydrate. The precipitating agents were sodium hydroxide and ammonium hydroxide, and the stabilizing agent was the pectin contained in the shell of the *Aloe vera* leaves for MDaloe, P1 and P2, and commercial pectin, also derived from *Aloe vera*, for MDpectin. The shell of the *Aloe vera* was selected as stabilizing agent because it is a commercially valuable and cheap waste resource that contains enough pectin in its leaves. Prior to the synthesis of these Fe-oxides, the cationic exchange capacity of the pectin was determined based on its available carbonyl groups. The experimental method used to do this was that reported by Norazelina Sah Mohd *et al.*, (2012). The ratios of total mmol total Fe / meq COO in the biomass (*i.e.* the pectin functional groups), used in the synthesis of MDaloe and MDpectin, were 106 and 170 respectively. In both cases the process was carried out with excess solution. These two samples look like a highly magnetic black powder with little or no remnants of the stabilizing organic matter. On the other hand, for the synthesis of P1 and P2, only an incipient volume of solution was used. The technique of incipient volume is applied here in order to reduce the total amount of solution to the minimum necessary to achieve the humidification of the material. This also avoids the formation of an excess of magnetite in the surplus solution that is not adsorbed by the pectin. In these samples, the ratios of total mmol total Fe / meq COO in the biomass were 8 (P1) and 11 (P2). The presence of the allegedly magnetite in P1 and P2 is not obvious to the naked eye. Indeed, their only visible parts are the remaining fibers of the *Aloe vera*, being P1 the only one attracted by a hand magnet.

Figures 1a and 1b show some SEM photomicrographs of the Fe-oxides, identified in samples MDaloe and MDpectin, with their corresponding EDX analyses. TEM photomicrographs of Fe-oxides, in P1 and P2, are presented in Figures 1c and 1d. From the SEM observations it is clear that some Fe-oxides, identified in sample MDaloe, show internal irregularities, namely lighter and darker regions within the same particle. According to the EDX analyses, the light regions are richer in Fe than the dark ones (Fig. 1a), which suggest that the Fe distribution may not be homogeneous because the Fe-rich particles (probably magnetite) are partially oxidized to maghemite or hematite. In fact, MDaloe shows, at first glance, a very slight reddish hue characteristic of hematite and/or maghemite. Another possibility to explain such heterogeneities is that the sample failed to aerate efficiently, generating various phases with different Fe content. The second SEM image, also for MDaloe (Fig. 1a), shows a euhedral cube, possibly magnetite. Opposite to MDaloe, the observed Fe oxides in MDpectin are more homogeneous (Fig. 1b), suggesting that the Fe binds uniformly to the commercial pectin. Thus, these differences between MDaloe and MDpectin, could be related to the purity of the stabilizing material. Indeed, the biomass in MDaloe is a mixture of organic compounds among which the pectin acts as the main stabilizing agent for Fe fixation. The rest of the biomass might have very variable composition, with a capacity to absorb the metal ions poorly understood so far. Instead, commercial pectin

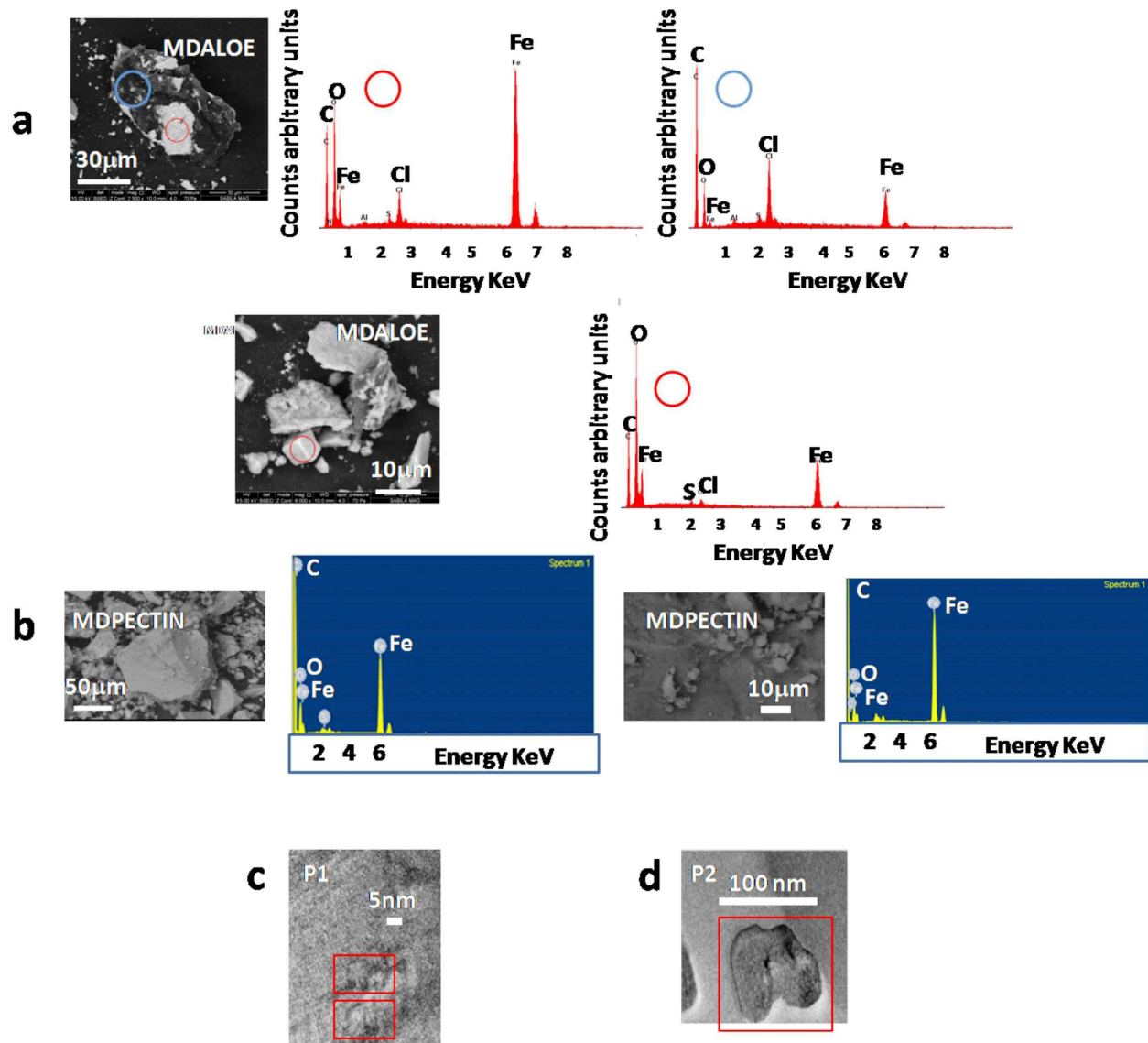


Figure 1. Scanning Electron Microscopy (SEM) photomicrographs of Fe-oxides, identified in samples MDaloe (a) and MDpectin (b), along with their corresponding X-Ray Energy Dispersion (EDX) analyses. Also shown: Transmission Electron Microscopy (TEM) photomicrographs of Fe-oxides identified in P1 (c) and P2 (d). For the first photomicrograph of MDaloe, the same particle of Fe-oxide is analyzed via EDX in both, the lighter (red circle) and darker (blue circle) regions, revealing different Fe content in each case. An euhedral cube (within the red circle) of what seems to be magnetite, is also shown in the second photomicrograph for this same sample. Scales indicate that MDaloe and MDpectin are large particles (few microns) of Fe-oxides, whereas P1 and P2 are within the nanometer range. Red squares in photomicrographs (c) and (d) frame the linear atomic series (darker areas) embedded in the pectin for P1 (metallic magnetite according to its XRD spectrum) and the amorphous Fe flakes for P2

is more pure, with no other agents that can impede the uptake of the Fe from the solution. For both, MDaloe and MDpectin, the Fe-oxide particles are several microns long. On the other hand, transmission electron microscopy (TEM) analyses (Figs. 1c and 1d) show, at an approximately 10 nm scale, linear atomic series embedded in the pectin for P1 (metallic magnetite according to its XRD spectrum) and weakly magnetized amorphous phases (flakes) of Fe oxides for P2.



3. Rock magnetic experiments

Thermosusceptibility and thermomagnetic curves (including low temperature measurements from 90K up), hysteresis loops, back field and isothermal remanent magnetization (IRM) acquisition curves were obtained for the four samples analyzed. Traditionally, highly sensitive (about 10^{-8} Am²/kg) susceptometers, alternating gradient force and superconducting quantum interference magnetometers have been widely used to measure susceptibility and magnetization (induced and remanent) of small amounts of synthetic Ti magnetites (*e.g.* Kaiser and Miskolczy 1970; Özdemir and Banerjee 1981; Amin *et al.*, 1987; Heider *et al.*, 1987; Zitzelsberger and Schmidbauer 1996; Almeida *et al.*, 2014 among others). However, in this study, the only equipment employed throughout all the experiments, was a versatile and unique Variable Field Translation Balance (VFTB), manufactured by Mag-Instruments UG (Munich, Germany), with sensitivity better than 10^{-6} Am²/kg. The operation principles of the VFTB are thoroughly described in Petersen and Petersen (2008).

The use of just one device, for the various experiments performed in this work, tremendously accelerates the measurement process. It also bypasses the repeated preparation of the same sample, to fit a variety of sample holders, which might be not only tedious, but also the source of possible experimental inaccuracies.

Due to the high sensitivity of the VFTB, 60 mg-sample of material was enough to reach sufficient accuracy in most of the experiments. The only exception was the weakly magnetized P2 in which case, thanks to the big capacity of the sample holder, we could use 100 mg in order to obtain an acceptable signal/noise ratio.

Thermosusceptibility and thermomagnetic heating and cooling cycles, as well as low temperature measurements (from 90 to 300 K) were performed in air atmosphere due to the lack of Argon at the very moment of running the experiments. However, the VFTB also allows for measurements in the Argon atmosphere, in order to reduce oxidation of the samples throughout heating.

All thermosusceptibility measurements were carried out with an initial small magnetic remanence, and no field applied throughout the experiment. On the other hand, the thermomagnetic curves were done in a low external field of 0.1 T. It is important to point out that the VFTB is the only device in the market capable of measuring simultaneously both, susceptibility and magnetization, in the same sample, during a complete temperature ramp. This feature might be quite useful since, in most cases, the results obtained from both experiments complement to each other.

Hysteresis loops (maximum range between -1000 and 1000 mT) and backfield coercivity measurements were carried out at room temperature. Isothermal remanent magnetization (IRM) acquisition curves were obtained for only few progressively increasing fields (about 10 points). However, not only the number and magnitude of the applied fields used in all measurements are fully customizable in the VFTB, but also the temperature of each experiment. The SIRMs for MDaloe and MDpectin were reached at 120 mT and 300 mT respectively.



4. Rock Magnetic characterization of the Fe-oxides: results and discussion

4.1 Magnetic Fe-oxides

The thermosusceptibility heating curve for MDaloe, shows some humps between 200° and 300° C, indicative of new magnetic minerals being formed. It also has a final drop just below 580° C typical of magnetite, preceded by a Hopkinson peak characteristic of fine-grained single domain (SD) and/or superparamagnetic (SP) magnetite (inset Fig. 2a). This same sample displays a considerably diminished susceptibility-cooling curve, suggesting some oxidation to hematite during heating. The cooling curve also shows complete reversibility of the Hopkinson peak (inset Fig. 2a). The presence of magnetite is confirmed by measuring magnetization versus heating, in a second run for that same sample (Fig. 2b).

The comparison between thermosusceptibility and thermomagnetic experiments in MDaloe, illustrates the advantages of the VFTB at measuring these two temperature ramps for the same sample. Indeed, the

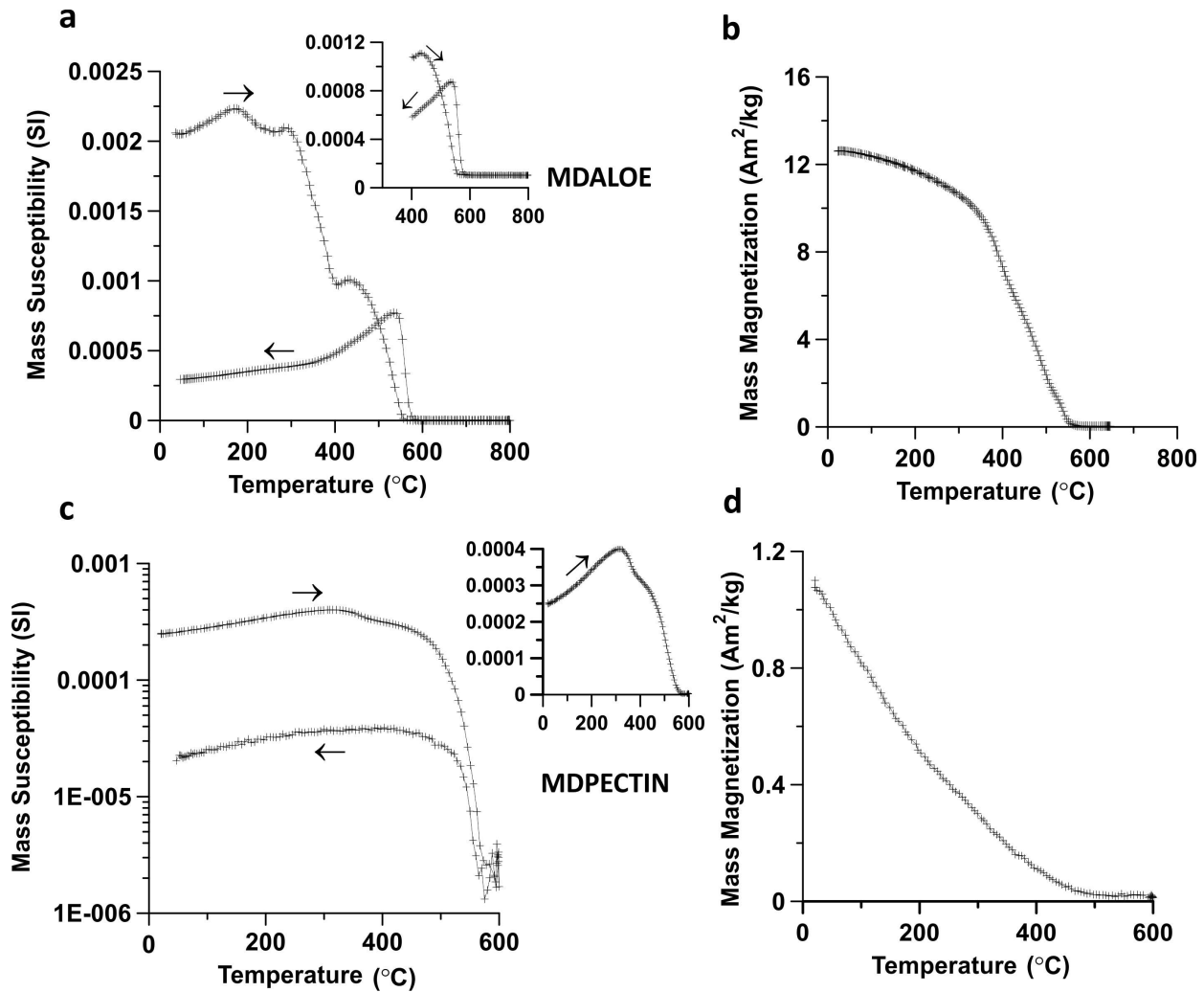


Figure 2. Thermosusceptibility cycles (heating and cooling) and themomagnetic curves of samples (a) and (b) MDaloe and (c) and (d) MDpectin respectively. The heating and cooling curves, in the thermosusceptibility cycle for MDaloe, show the reversibility of a Hopkinson peak just below 580°C (inset in a). The heating curve, in the thermosusceptibility cycle for MDpectin, shows the presence of maghemite with a possible maghemite/hematite thermal transition between 200° and 300° C (inset in c).



differences between the two curves exemplifies the behavior of a set of dispersed fine-grained magnetite, in presence of a low field, over a narrow range of temperatures just below 580° C. In such a range, which marks the transition between stable SD to the SP state, the spontaneous magnetization is still present and decreases with an increase of the temperature as shown in Figure 1b. At the same time, there is a sharp drop of the anisotropies that influence the direction of this magnetization, with the consequent Hopkinson peak displayed by the magnetic susceptibility in Figure 1a (Pfeiffer and Schiippel, 1994; Sláma *et al.*, 2011).

The susceptibility heating-curve for MDpectin has a conspicuous temperature transition within the 200°-300° C interval, as well as a magnetite drop at 580° C (Fig. 2c). Once more, evidence for hematite formation comes from the much lower susceptibility values displayed by the magnetite-like cooling-curve, which opposite to MDaloe does not have a marked SD/SP Hopkinson peak. A second temperature ramp (Fig. 2d), carried out on this same sample, and measuring magnetization throughout heating, shows a paramagnetic component (Langevin-like magnetic response) that seems to dominate the antiferromagnetic and ferrimagnetic fractions (*i.e.* hematite and magnetite).

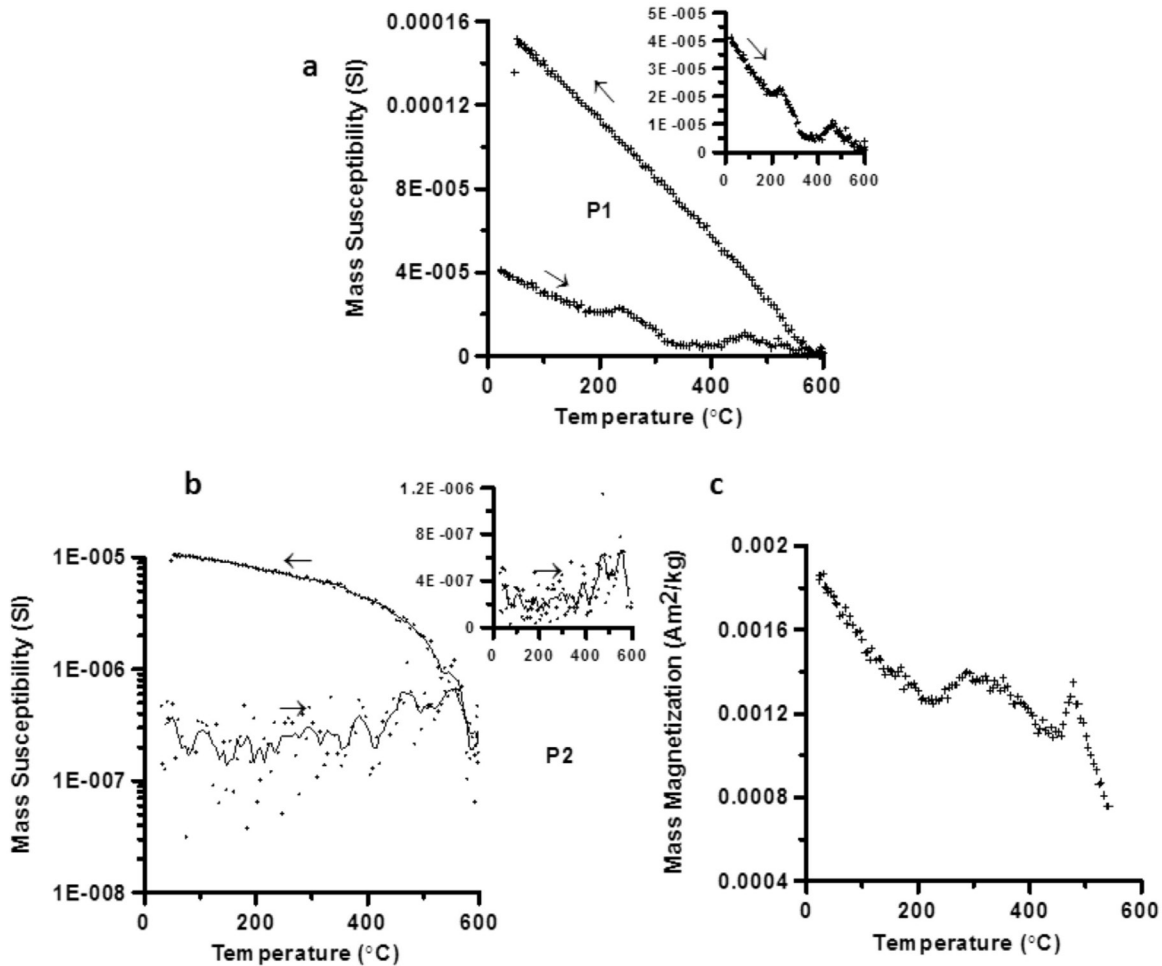


Figure 3. Thermosusceptibility cycles (heating and cooling) and thermomagnetic curves for samples (a) P1 and (b) and (c) P2 respectively. The heating curves in the thermosusceptibility cycle of P1 y the thermomagnetic curve of P2 show the presence of maghemite with a possible maghemite/hematite thermal transition between 200° and 300° C (inset in a). The dynamic range of the Variable Field Translation Balance (VFTB), used in these measurements, is challenged by P2, with a roughly defined fine-grained SD/SP Hopkinson peak at ca 580°C, in the thermosusceptibility heating curve (inset in b).



The susceptibility heating-curve for P1 also displays a hump between 200° and 300° C and a small Hopkinson peak at about 580° C, revealing the presence of a SD/SP fraction (Fig. 3a). In addition, this curve shows a Langevin-like component superimposed to the antiferromagnetic and ferrimagnetic signals. The thermosusceptibility cycle is irreversible, with a cooling curve dominated by the presence of magnetite without a Hopkinson peak.

Finally, sample P2 has a very low and noisy susceptibility heating curve, with a roughly defined fine-grained SD/SP magnetite Hopkinson peak, as well as a characteristic and irreversible magnetite cooling-curve (Fig. 3b). However, a magnetization versus temperature ramp, for a different sample from the same P2 material, yields a clear cut curve with a considerable paramagnetic fraction (Langevin-like curve) overlapping the same 200° to 300° C temperature transition observed in the rest of the samples, plus a magnetite (*i.e.* 580° C drop) signal. It is noteworthy that the dynamic range of the VFTB is successfully tested by P2, allowing a satisfactory separation of the susceptibility signal from the noise level.

The transition between 200° and 300° C, revealed in MDaloe, MDpectin and P1 thermosusceptibility and P2 thermomagnetic curves, could be due to either Ti magnetite or to inversion of maghemite to hematite via annealing of defects and internal stress (Figs. 2 and 3). Such a transition might also depend on grain size and impurities in maghemite (*e.g.* Liu *et al.*, 2005; Liu *et al.*, 2010). The only possible source of Ti in these samples, to form Ti magnetite, would be the plant-extracted pectin. However, the average content of Ti in plants is rather low, ranging between 0.02 and 56 mg/kg (Markert, 1992). Thus, the presence of maghemite, appears to be the more likely explanation for such a transition. Indeed, it is noticeable that, during the synthesis of P1 and P2, the color of the organic tissues went from black to sandy brown. This change might be indicative of the formation of some other Fe species, besides magnetite, in an oxidizing atmosphere.

The low reversibility level of the thermosusceptibility curves for the MD (*i.e.* aloe and pectin) and the P (1 and 2) samples, are particularly noteworthy. The first two ones, with very little remnants of the pectin matrix, show a large decrease of the susceptibility during heating (Figs. 2a and 2c), due perhaps to a simple transformation of maghemite and magnetite to hematite. On the other hand, the increase of susceptibility in P1 and P2 (*i.e.* Figs. 3a and 3b), which have a high content of the pectin remnants, could be explained as the subsequent reduction of some hematite to magnetite throughout heating, in presence of abundant organic matter (Hanesch *et al.*, 2006). The level of oxidation after heating, in all these samples, also increases in direct proportion to the high surface area/volume ratio that characterizes fine-grained microscopic magnetite particles, which is particularly noteworthy in P1 and P2.

For the analysis of the IRM acquisition curves, obtained for MDaloe and MDpectin, we used a method based on a Direct Signal Analysis (DSA) (Aldana *et al.*, 1994; Aldana *et al.*, 2011 and Rada *et al.*, 2011). Figure 4 shows these two curves, along with their fittings, after applying the DSA. The Figure also displays the spectral histograms and the adjusted Gaussian envelopes with $\log B_{1/2}$ centers at about 1 and 1.3. These values correspond to those magnetic phases with the lowest remanent acquisition coercivities, namely magnetite and/or maghemite (Peters and Dekkers, 2003).

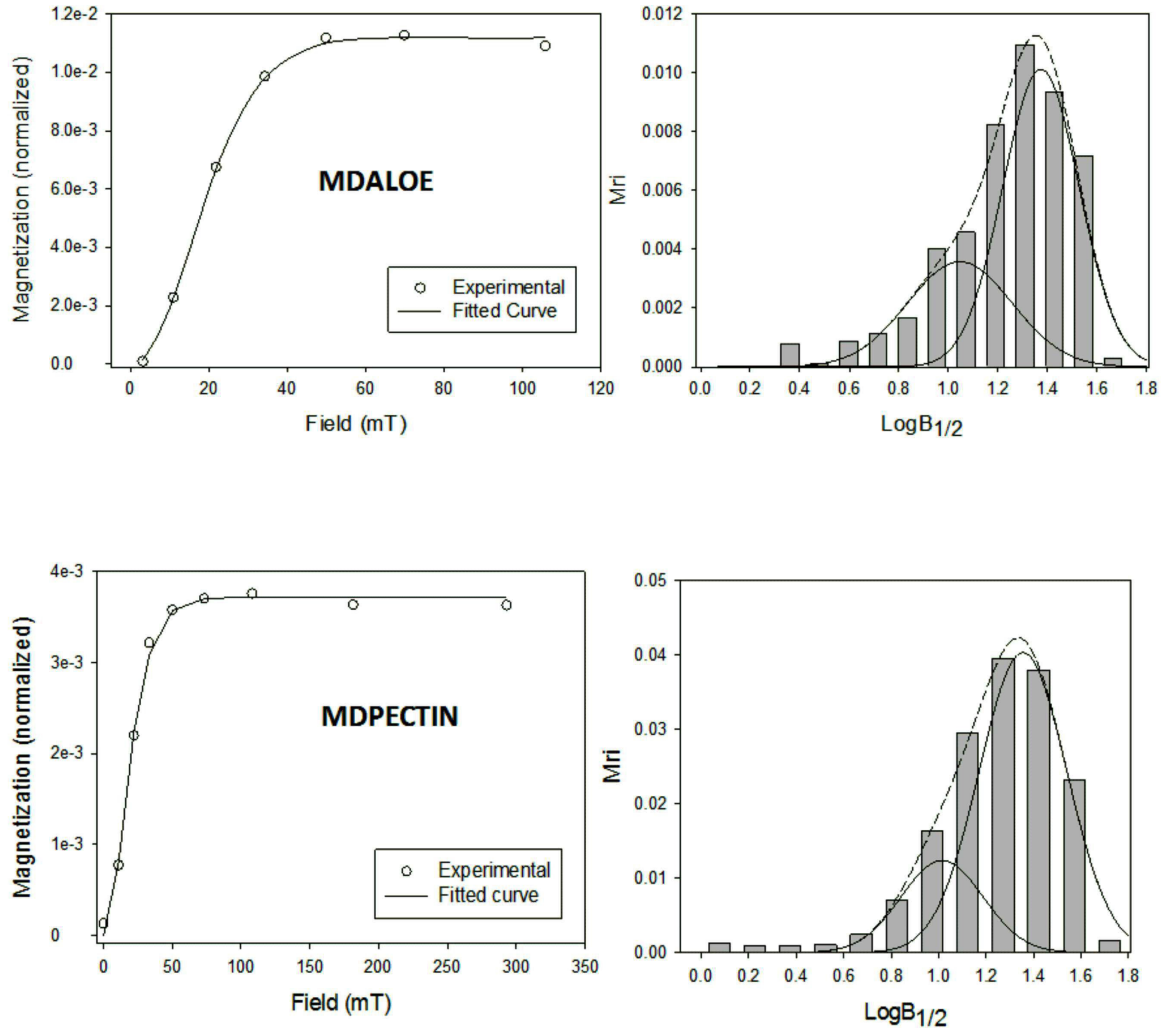


Figure 4. Direct Signal Analysis decomposition of the IRM curves for MDaloe and MDpectin. In each case, the experimental data (open circles) and the results of the DSA fitting (smooth line) are presented. Also shown: the resulting spectral histograms and the adjusted Gaussian envelopes, corresponding to the two magnetic phases identified in these samples. The dashed lines on the histograms are the whole envelopes, namely the sum of the Gaussian curves corresponding to each magnetic phase (*i.e.* continuous lines). The $\log B_{1/2}$ centers of the Gaussian envelopes are about 1 and 1.3 for both MDaloe and MDpectin. These $\log B_{1/2}$ values might correspond to the presence of both magnetite and/or maghemite.

Low temperature magnetic remanence analyses, carried out by progressive warming up of these four samples (*i.e.* from 90 to 300K), show a rather noisy signal (Fig. 5). However, from these curves, it is clear that the Verwey transition (*i.e.* ca 110K), typical of magnetite, is largely suppressed in MDaloe and MDpectin, and fully suppressed in P1 and P2 (insets Fig. 5). This result suggests that these samples undergone almost complete oxidation to maghemite (Özdemir *et al.*, 1993). However, the samples should also have smaller amounts of residual magnetite, according to the results of the other rock magnetic analysis. The warming curves for MDaloe and MDpectin are slightly humped just above 110 K, compared to their P1 and P2 counterparts that are not humped at all (insets of Fig. 5). This could be due to the different oxidation states of each sample, namely the latter two would be much more maghemitized than the first ones (Özdemir and Dunlop, 2010).

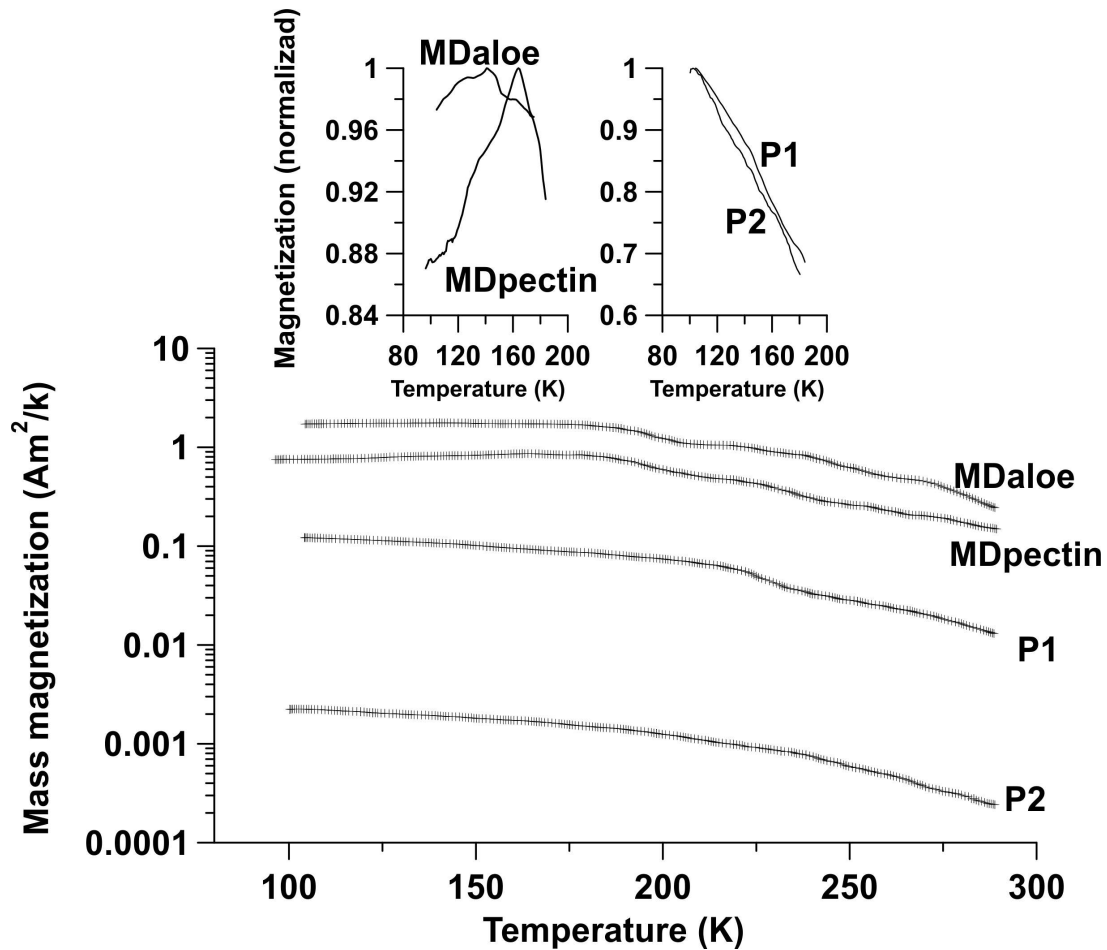


Figure 5. Normalized remanence curves for the four samples analyzed throughout warming up to 300 K. The insets show the hump-like forms of the warming curves, above the Verwey transition, for samples MDaloe and MDpectin. They also show the suppression of this transition in P1 and P2, suggesting an almost complete oxidation of these samples to maghemite.

Thermosusceptibility and themoremanence experiments, carried out in air atmosphere, might account for some oxidation of these Fe oxides throughout heating at high temperatures. However, IRM and low temperature experiments suggest the presence of maghemite in the unheated samples too.

4.2 Magnetic particles: sizes and shapes

Figure 6 shows the hysteresis loops for the four samples analyzed. They are steep, narrow and closed, approaching to saturation at fields of about 450 mT for MDaloe, 800 mT for MDpectin, over 600 mT for P1 and over 1000 mT for P2. Their shapes reveal the dominant presence of low coercivity magnetic phases (*i.e.*

Table 1. Hysteresis parameters of the four samples analyzed.

| | Mrs(Am ² /kg) | Ms(Am ² /kg) | Mrs/Ms | Hcr (mT) | Hc (mT) | Hcr/Hc |
|-----------------|--------------------------|-------------------------|--------|----------|---------|--------|
| MDaloe | 0.929 | 31.322 | 0.03 | 13 | 0.168 | 77.38 |
| MDpectin | 0.354 | 24.9 | 0.014 | 14 | 0.107 | 131 |
| P1 | 0.084 | 3.248 | 0.026 | | 0.288 | |
| P2 | 0.001 | 1.63E-02 | 0.061 | | 10 | |

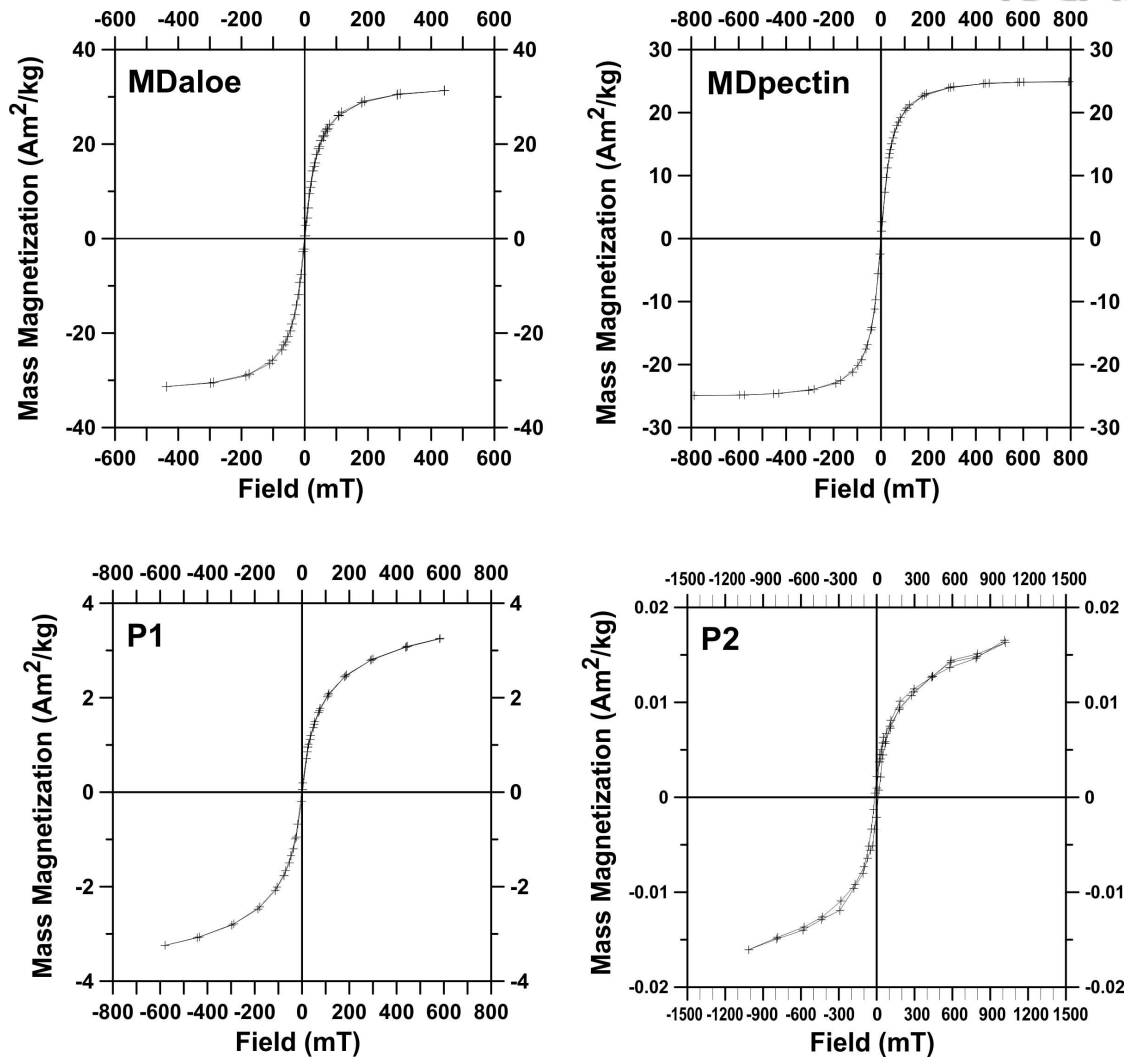


Figure 6. Hysteresis loops, for the four samples analyzed. These loops are steep, narrow and closed, revealing the dominant presence of a low coercivity magnetic phase that could be multidomain (MD) magnetite in MDaloe and MDpectin, or fine-grained single domain (SD) magnetite and/or superparamagnetic (SP) magnetite in P1 and P2.

MD or small SD magnetite close to the SD/SP threshold). Dipolar interactions between SP particles might also result into the small remanence (M_{rs}), coercivity (H_c) and squareness (M_{rs}/M_s) values observed for these samples (Chiolerio *et al.*, 2014). Only for MDaloe and MDpectin it was possible to measure IRM and backfield coercivity, since for P1 and P2 the IRMs were below the noise level of the VFTB.

We plotted squareness (M_{rs}/M_s) and coercivity of remanence - coercive force (H_{cr}/H_c) ratios for MDaloe and MDpectin in a Day plot (Table 1 and Fig. 7a). Both of them appear to be mostly MD magnetite. In fact, SEM analyses for these two samples show that they are composed mainly by clustered large-grained Fe-oxides over $10 \mu\text{m}$ (Figs. 1a and 1b).

On the other hand, for P1 and P2, TEM analyses show Fe-oxides at an approximately 10 nm scale (Figs. 1c and 1d). These observations, together with the impossibility of measuring the H_{cr} and the anomalously low M_{rs} and H_c of these two samples, suggest that they might contain SP and/or fine-grained SD magnetite, with grain sizes close to the SD/SP threshold. Dipolar interactions between these particles seem unlikely due to the undersaturated solution of total metallic charge used to synthesize P1 and P2.

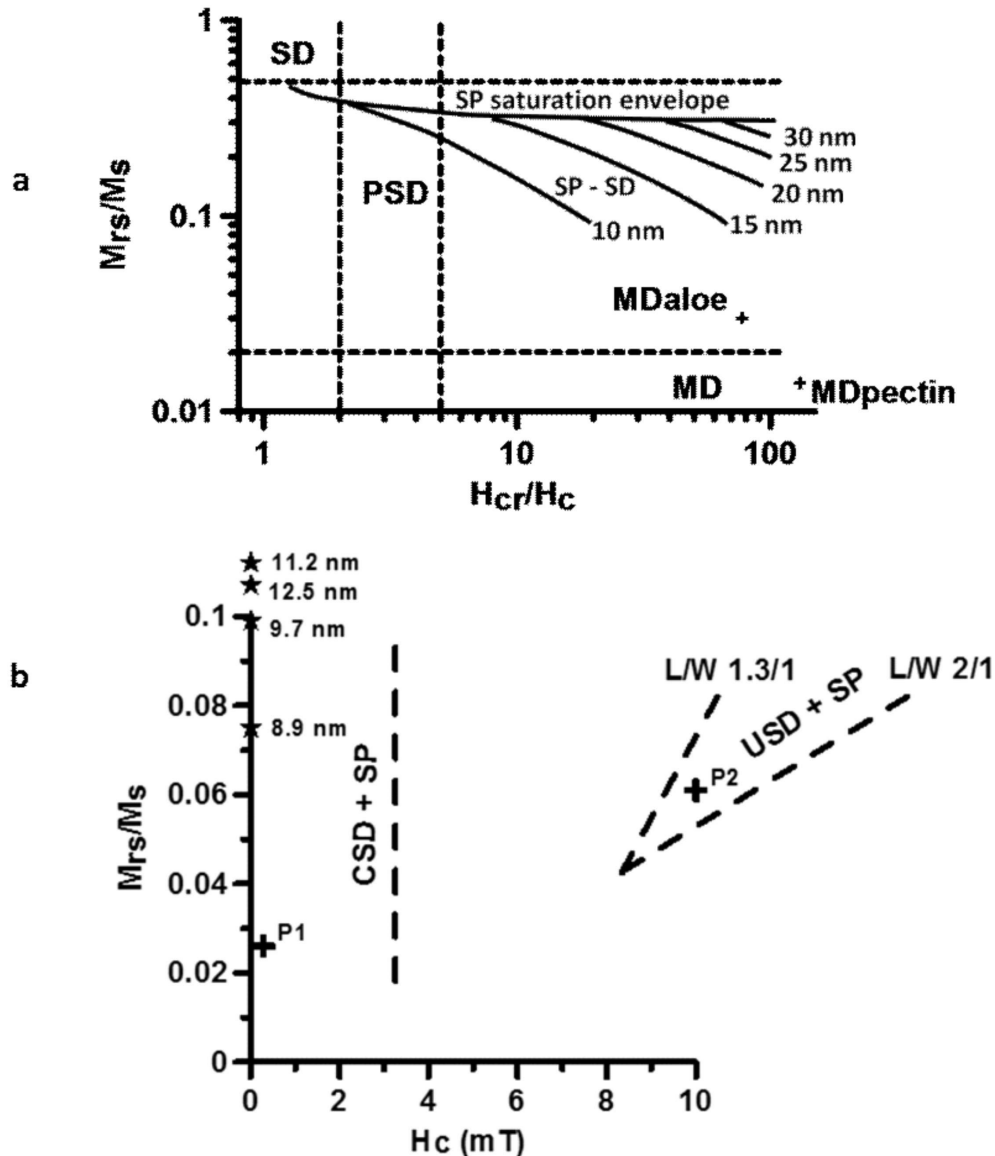


Figure 7. Hysteresis parameters from Table 1 are plotted for: a) MDaloe and MDpectin against the theoretical Day plot curves calculated for magnetite (after Dunlop, 2002), in mixtures of soft (SP and MD) and hard SD grains (*i.e.* numbers along the curves show the grain sizes) and b) P1 and P2 against the theoretical predictions of squareness (M_{rs}/M_s) and coercive field H_c calculated for randomly oriented populations of dispersed and uniformly magnetized magnetite (after Tauxe *et al.*, 2002). USD + SP is the region corresponding to predicted mixtures of SP and uniaxial single domain magnetite with length to width ratios (L/W) ranging from 1.3 to 2. The CSD +SP line defines the hypothetical region for mixtures of cubic single domain and SP magnetite. The stars are the hysteresis parameters of four different-size magnetite nanoparticles, synthesized from iron sands by coprecipitation (after Sunaryono *et al.*, 2015).

In Figure 7b, the hysteresis parameters of P1 and P2 (*i.e.* M_{rs}/M_s and H_c from Table 1) are plotted against the theoretical predictions of squareness and coercive fields for randomly oriented populations of dispersed and uniformly magnetized magnetite (Tauxe *et al.*, 2002). P1 lies in the region for fine-grained (close to the SD/SP threshold) of cubic (isotropic) magnetite, whereas P2 lies in the field corresponding to a mixture of uniaxial SD and SP magnetite (*i.e.* acicular). By way of comparison, the squareness and H_c of five nanomagnetites in the SD/SP threshold, synthesized by co-precipitation of iron sands (Sunaryono *et*



al., 2015), are also plotted in the same figure. The observed trend in these samples is an increase of M_s and M_{rs} with particle size, in the stable SD region. A word of caution should be stressed about the value of H_c obtained for P2 (Table 1 and Fig. 7b) though. In fact, according to the hysteresis loops of Figure 6, the mass magnetization measured for this sample is two orders of magnitude lower than those measured for P1. Therefore, the sensitivity of the VFTB is challenged to its limits, with a likely inaccurate determination of the H_c value, two orders of magnitude higher than its P1 counterpart.

According to Foba-Tendo *et al.*, (2013), the carboxyl groups of the pectins seem to be the focal points for the formation of the synthesized Fe-oxides. The vibrational bands of the infrared spectrum, corresponding to these carboxyl groups, are more stretched in P2 than in P1. In the case of P2, the mmol total Fe / meq COO ratio in the biomass (*i.e.* 14) is almost twice that of P1 (*i.e.* 8), which would indicate a higher interaction of the Fe ions with these exchange sites. Thus, the distinct experimental conditions used to synthesize P1 and P2 would alter the biomass in a different way and, as a consequence, they would also might have an effect on the separation between the available spaces in the pectin, for the localization of the Fe oxides. Hence, it would be possible to argue that the mmol total Fe / meq COO ratios in the biomass might have conditioned somehow the growth, ordering and geometry of the magnetite crystals. At the end, this could have affected the M_{rs}/M_s and H_c values measured for these samples.

5. Conclusions

A preliminary rock magnetic characterization of some Fe-oxides, synthesized at room temperature via co-precipitation of ferric chloride and ferrous sulfate hexahydrate precursors, in pectins from *Aloe vera*, makes it possible to inquire about their nature, state of oxidation, size and approximate shapes.

Thermomagnetic and thermosusceptibility curves test positive for magnetite in all the samples. Maghemite seems to be also present with a characteristic thermal transition between 200° and 300° C. In MDaloe and MDpectin, with little remnants of biomass, maghemite appears to have inverted to hematite throughout heating without further changes (*i.e.* decrease of susceptibility values in the cooling curve). On the other hand, the resulting hematite in P1 and P2, reduces to magnetite in presence of organic matter (increase of susceptibility values in the cooling-curve). Oxidation to maghemite was favored perhaps by the high surface area/volume ratio of these microscopic magnetite particles. The Hopkinson peaks, around 580° C, observed in the themosusceptibility curves of some of these samples, reveal the presence of SP or fine-grained SD magnetites. In addition, the analysis of the IRM curves unfolds the presence of only low coercivity magnetic phases (*i.e.* magnetite and/or maghemite), whereas the low temperature experiments suggest that MDaloe, MDpectin, P1 and P2 have been largely maghemitized at different levels.

All the hysteresis loops show very low M_{rs} and H_c values, characteristic of either dipolar interactions between fine-grained magnetite particles, MD magnetite and/or small magnetites around the SD/SP threshold. SEM observations and M_{rs}/M_s and H_{rc}/H_c ratios for samples MDaloe and MDpectin suggest that they are mostly MD domain magnetites. On the other hand, the M_{rs}/M_s and H_c values for P1 and P2, plotted



against the theoretical predictions of squareness and coercive fields for SD magnetite, seem to imply that these two samples have magnetite particle sizes around the SD/SP threshold (about 10 nm), with cubic (P1) and acicular (P2) shapes. Furthermore, the different mmol total Fe / meq COO ratios in the biomass, used to their synthesis, appear to have conditioned the growth, ordering and geometry of these magnetic crystals.

Acknowledgments

We are grateful to Professor Stuart Gilder from Institute for Geophysics, LMU in Munich for providing access to VFTB on which the sample's measurements were performed.

References

- Aldana M., Laredo E., Bello A., Suarez N., 1994. Direct signal analysis applied to the determination of the relaxation parameters from TSDC spectra of polymers. *J. Polym. Sci. Polym. Phys.* 32, 2197 – 2206.
- Aldana M., Costanzo-Álvarez V., Gómez L., González C., Díaz M., Silva P., Rada M., 2011. Identification of magnetic minerals related to hydrocarbon authigenesis in Venezuelan oil fields using an alternative decomposition of isothermal remanence curves. *Stud Geophys Geod* 55, 343 – 358.
- Almeida T.P., Muxworthy A.R., Williams W., Kasama T., Dunin-Borkowski R., 2014. Magnetic characterization of synthetic titanomagnetites: Quantifying the recording fidelity of ideal synthetic analogs. *Geochem. Geophys. Geosy.* 15, 161 – 175. DOI: 10.1002/2013GC005047
- Amin N., Arajs S., Matijevi E., 1987. Magnetic properties of uniform spherical magnetite particles prepared from ferrous hydroxide gels, *Phys. Stat. Solidi A* 101, 233 – 238.
- Bharde A., Wani A., Shouche Y., Joy P.A., Prasad B.L.V., Sastry M., 2005. Bacterial Aerobic Synthesis of Nanocrystalline Magnetite. *J. Am. Chem. Soc.* 127, 9326 – 9327. DOI: 10.1021/ja0508469
- Bharde A., Rautaray D., Bansal V., Ahmad A, Sarkar I., Mohammad Yusuf S., Sanyal M., Sastry M., 2006. Extracellular Biosynthesis of Magnetite using Fungi. *Small* 2, 135 – 141. DOI: 10.1002/smll.200500180
- Cai Y., Shen Y., Xie A., Li S., Wang X., 2010. Green synthesis of soya bean sprouts-mediated superparamagnetic Fe₃O₄ nanoparticles. *J. Magn. Magn. Mater* 322, 2938 – 2943.
- Chhabra V., Ayyub P., Chattopadhyay S., Maitra A.N., 1996. Preparation of acicular γ -Fe₂O₃ particles from a microemulsion-mediated reaction. *Mater Lett.* 26, 21 – 26.
- Chikazumi S., Taketomi S., Ukita M., Mizukami M., Miyajima H., Setogawa M., Kurihara Y., 1987. Physics of magnetic fluids. *J. Magn. Magn. Mater* 65, 245 – 251.
- Chiolerio A., Chiodoni A., Allia P., Martino P., 2014. Magnetite and Other Fe-Oxide Nanoparticles. In: (Bhushan B., Luo D., Schrickler S.R., Sigmund W., Zauscher S., eds.) Handbook of Nanomaterials Properties. Springer-Verlag Berlin Heidelberg, pp 213 – 246. DOI 10.1007/978-3-642-31107-9_34.
- Chowdhury S.R., Yanful E.K., Pratt A.R., 2010. Arsenic removal from aqueous solutions by mixed magnetite-maghemite nanoparticles. *Environ Earth Sci* DOI 10.1007/s12665-010-0865-z
- Chowdhury S.R., Yanful E.K., 2013. Kinetics of cadmium (II) uptake by mixed maghemite-magnetite nanoparticles. *J. Environ. Manage* 129, 642 – 51. DOI: 10.1016/j.jenvman.2013.08.028.
- Daichuan D., Pinjie H., Shushan D., 1995. Preparation of uniform β -FeO(OH) colloidal particles by hydrolysis of ferric salts under microwave irradiation. *Mater Res. Bull.* 30, 537 – 541.



- Deng Y., Wang L., Yang W., Fu S., Elaïssari A., 1999. Preparation of magnetic polymeric particles via inverse microemulsion polymerization process. *J. Magn. Magn. Mater* 257, 69 – 78.
- Dunlop D.J., 2002. Theory and application of the Day plot (Mrs/Ms versus Hcr/Hc) 1. Theoretical curves and tests using titanomagnetite data. *J. Geophys. Res.* doi:10.1029/2001JB000486
- Elliott D.W, Zhang W-X., 2001. Field Assessment of Nanoscale Bimetallic Particles for Groundwater Treatment. *Environ. Sci. Technol.* 35, 4922 – 4926 DOI: 10.1021/es0108584
- Foba-Tendo J. Ngenefeme, Namanga J. Eko, Yufanyi D. Mbom, Ndinteh D. Tantoh, Krause W.M. Rui., 2013. A One Pot Green Synthesis and Characterization of Iron Oxide-Pectin Hybrid Nanocomposite. *J. Compos. Mater.* 3, 30 – 37.
- Giraldo L., Erto A., Moreno-Piraján J.C., 2013. Magnetite nanoparticles for removal of heavy metals from aqueous solutions: synthesis and characterization. *Adsorption* 19: 465 – 474: DOI 10.1007/s10450-012-9468-1
- Gonzalez-Catteno T., Morales M.P., Gracia M., Serna C.J., 1993. Preparation of uniform γ -Fe₂O₃ particles with nanometer size by spray pyrolysis. *Mater Lett.* 18, 151 – 155.
- Gupta A.K., Gupta M., 2005. Synthesis and surface engineering of iron oxide nanoparticles for biomedical applications. *Biomaterials* 26, 3995 – 4021.
- Hanesch M., Stanjek H., Petersen N., 2006. Thermomagnetic measurements of soil iron minerals: the role of organic carbon, *Geophys, J, Int*, 165, 53 – 61.
- Heider F., Dunlop D.J, Sugiura N., 1987. Magnetic properties of hydrothermally recrystallized magnetite crystals. *Science* 236, 1287 – 1290.
- Hyeon T., 2003. Chemical synthesis of magnetic nanoparticles. *Chem Commun* 8: 927 – 934.
- Kaiser R., Miskolczy G., 1970. Magnetic Properties of Stable Dispersions of Subdomain Magnetite Particles. *J. Appl. Phys.* 41, 1064 – 1072 DOI: <http://dx.doi.org/10.1063/1.1658812>
- Kang Y.S., Risbud S., Rabolt J.F., Stroeve P., 1996. Synthesis and characterization of nanometer-size Fe₃O₄ and γ Fe₂O₃ particles. *Chem. Mater.* 8, 2209 – 2211.
- Kenawy E.R., Kamoun E.A., Mohy Eldin M.S., El-Meligy M.A., 2014. Physically cross linked poly (vinyl alcohol)-hydroxyethyl starch blend hydrogel membranes: Synthesis and characterization for biomedical applications. *Arab. J. Chem.* 7, 372 – 380.
- Kim J., Piao Y., Hyeon T., 2009. Multifunctional nanostructured materials for multimodal imaging, and simultaneous imaging and therapy. *Chem. Soc. Rev.* 38, 372 – 390. DOI: <http://dx.doi.org/10.1039/b709883a>
- Lang C., Schuler D., Faivre D., 2007. Synthesis of Magnetite Nanoparticles for Bio- and Nanotechnology: Genetic Engineering and Biomimetics of Bacterial Magnetosomes. *Macromol. Biosci.* 7, 144 – 151
- Lao L.L., Ramanujan R.V., 2004. Magnetic and hydrogel composite materials for hyperthermia applications. *J. Mater. Sci. Mater. Med.* 15, 1061 – 1064.
- Li Y., Liao H., Qian Y., 1998. Hydrothermal Synthesis of Ultrafine α -Fe₂O₃ and Fe₃O₄ Powders. *Mater Res, Bull*, 33, 841 – 844.
- Liu Q.S., Deng C.L., Yu Y., Torrent J., Jackson M.J., Banerjee S.K., Zhu R., 2005. Temperature dependence of magnetic susceptibility in an argon environment: Implications for pedogenesis of Chinese loess/palaeosols. *Geophys, J, Int*, 161, 102 – 112. DOI: 10.1111/j.1365-246X.2005.02564.x



- Liu X.M., Shaw J., Jiang J.Z., Bloemendal J., Hesse P., Rolph T., Mao X.G., 2010. Analysis on variety and characteristics of maghemite. *Sci. China Earth Sci.* 53, 1153 – 1162. doi:10.1007/s11430-010-0030-2
- Liu Ch-H., Chuang Y.-H., Chen T.-Y., Tian Y., Li H., Wang M.-K., and Zhang W., 2015. Mechanism of Arsenic Adsorption on Magnetite Nanoparticles from Water: Thermodynamic and Spectroscopic Studies. *Environ. Sci. Technol.* 49, 7726 – 7734. DOI: 10.1021/acs.est.5b00381
- Lu A.-H., Salabas E.L., Schuth F., 2007. Magnetic Nanoparticles: Synthesis, Protection, Functionalization, and Application. *Angew. Chem. Int. Ed.* 46, 1222 – 1244.
- Markert B., 1992. Presence and significance of naturally occurring chemical elements of the periodic system in the plant organism and consequences for future investigations on inorganic environmental chemistry in ecosystems. *Vegetation* 103, 1 – 30.
- Massart R., 1981. Preparation of aqueous magnetic liquids in alkaline and acidic media. *IEEE Trans. Magn.* 17, 1247 – 1248.
- Mendoza Zélis P., Muraca D., Gonzalez J.S., Pasquevich G.A., Alvarez V.A., Pirota K.R., Sánchez F.H., 2013. Magnetic properties study of iron-oxide nanoparticles/PVA ferrogels with potential biomedical applications. *J. Nanoparticle Res.* 15, 1613 – 1616.
- Mornet S., Vasseur S., Grasset F., Verveka P., Goglio G., Demourgues A., Portier J., Pollert E., Duguet E., 2006. Magnetic nanoparticle design for medical applications. *Prog. Solid State Chem.* 34, 237 – 247.
- Norazalina Sah Mohd I., Nazaruddin R., Norziah Mohd H., Zainudin M., 2012. Extraction and Characterization of Pectin from Dragon Fruit (*Hylocereus polyrhizus*) using various extraction conditions. *Sains Malaysiana* 41(1), 41 – 45.
- Nyiro-Kosa I., Nagy D.C., Posfai M., 2009. Size and shape control of precipitated magnetite nanoparticles. *Eur. J. Mineral* 21, 293 – 302.
- Özdemir Ö., Banerjee S.K., 1981. An experimental study of magnetic viscosity in synthetic monodomain titanomagnetite: Implications for the magnetization of the ocean crust. *J. Geophys. Res.* 86, 11,864 – 11, 868
- Özdemir Ö., Dunlop DJ, Moskowitz BM., 1993. The effect of oxidation on the Verwey transition in magnetite. *Geophys. Res. Lett.* 20, 1671 – 1674, doi:10.1029/93GL01483.
- Özdemir Ö., Dunlop D., 2010. Hallmarks of maghemitization in low-temperature remanence cycling of partially oxidized magnetite nanoparticles. *J. Geophys. Res.* 115, B02101, doi:10.1029/2009JB006756
- Pankhurst Q.A., Connolly J, Jones SK, Dobson J., 2003. Applications of magnetic nanoparticles in biomedicine. *J. Phys. D. Appl. Phys.* 36, R167. <http://dx.doi.org/10.1088/0022-3727/36/13/201>
- Perez-González T., Rodríguez-Navarro A., Jiménez-López C., 2011. Inorganic Magnetite Precipitation at 25 degrees C: A Low-Cost Inorganic Coprecipitation Method. *J. Supercond. Nov. Magn.* 24, 549 – 557.
- Peters C., Dekkers M.J., 2003. Selected room temperature magnetic parameters as a function of mineralogy, concentration and grain size. *Phys. Chem. Earth* 28, 659 – 667.
- Petersen N., Petersen K., 2008. Comparison of the temperature dependence of irreversible and reversible magnetization of basalts. *Phys. Earth Planet. In.* 169, 89 – 91.
- Pfeiffer H., Schiippel W., 1994. Temperature dependence of the magnetization in fine particle systems and the Hopkinson effect. Application to barium ferrite powders. *J. Magn. Magn. Mater.* 130, 92 – 98.



- Philip D., 2009. Biosynthesis of Au, Ag and Au-Ag nanoparticles using edible mushroom extract. *Spectrochim Acta* 73, 374–381 DOI: 10.1016/j.saa.2009.02.037
- Priya James H., John R., Alex A., Anoop K.R., 2014. Smart polymers for the controlled delivery of drugs – a concise overview. *Acta Pharm. Sin. B.* 4, 120 – 127.
- Qu S.C., Yang H.B., Ren D.W., Kan S.H., Zou G.T., Li D.M., Li M.H., 1999. Magnetite nanoparticles prepared by precipitation from partially reduced ferric chloride aqueous solutions. *J. Colloid Interface Sci.* 215, 190 – 192.
- Rada Torres M.A., Costanzo-Álvarez V., Aldana M., Suárez N., Campos C., Mackowiak-Antczak M.M., Brandt M.C., 2011. Petrographic, rock magnetic and dielectric characterization of prehistoric Amerindian potsherds from Venezuela. *Stud. Geophys. Geod.* 55, 717 – 736. doi:10.1007/s11200-010-9021-1
- Ramanujan R.V., Lao L.L., 2006. The mechanical behavior of smart magnet–hydrogel composites. *Smart Mater. Struct.* 15, 952 – 956.
- Sahoo Y., Pizem H., Fried T., Golodnitsky D., Burstein L., Sukenik C.N., and Markovich G., 2001. Alkyl phosphonate/phosphate coating on magnetite nanoparticles: a comparison with fatty acids. *Langmuir* 17, 7907 – 7911.
- Shiple H.J., Yean S., Kan A.T., Tomson M.B., 2009. Adsorption of Arsenic to Magnetite Nanoparticles: Effect of Particle Concentration, Ph, Ionic Strength, and Temperature. *Environ. Toxicol. Chem.* 28, 509 – 515.
- Shubayev VI, Pisanic II T.R., Jin S., 2009. Magnetic nanoparticles for theragnostics. *Adv Drug Deliver Rev.* 61, 467-477. DOI: <http://dx.doi.org/10.1016/j.addr.2009.03.007>
- Sensenig R., Sapir Y., MacDonald C., Cohen S., Polyak B., 2012. Magnetic nanoparticle-based approaches to locally target therapy and enhance tissue regeneration in vivo. *Nanomedicine-UK* 7:1425 – 1442. DOI: <http://dx.doi.org/10.2217/nnm.12.109>
- Sláma J., Šoka M., Grusková A., González A., Jančárik V., 2011. Hopkinson effect study in spinel and hexagonal ferrites. *J. Electr. Eng.* 62, 239 – 243.
- Sunaryono, Ahmad Taufiq, Mashuri, Suminar Pratapa, Zainuri M., Triwikantoro, Darminto, 2015. Various Magnetic Properties of Magnetite Nanoparticles Synthesized from Iron-sands by Coprecipitation Method at Room Temperature. *Materials Science Forum* 827, 229 – 234. doi:10.4028/www.scientific.net/MSF.827.229
- Tang J., Myers M., Bosnick K.A., Brus L.E., 2003. Magnetite Fe₃O₄ nanocrystals: spectroscopic observation of aqueous oxidation kinetics. *J. Phys. Chem. B*, 107: 7501 – 7506.
- Tauxe L., Neal Bertram H., Seberino C., 2002. Physical interpretation of hysteresis loops: Micromagnetic modeling of fine particle magnetite. *Geochem. Geophys. Geosyst.* 3(10), 1055, doi:10.1029/2001GC000241
- Visalakshi G. Venkateswaran G., Kulshreshtha S.K., Moorthy P.H., 1993. Compositional characteristics of magnetite synthesized from aqueous solution at temperatures up to 523 K. *Mat. Resource Bull.* 28, 829 – 836.
- Worm H.-U., Markert H., 1987. The preparation of dispersed titanomagnetite particles by the glass-ceramic method. *Phys. Earth Planet. Inter.* 46, 263 – 270
- Zahn M., 2001. Magnetic Fluid and Nanoparticle Applications to Nanotechnology. *J. Nanoparticle Res.* 3, 73 – 78.



- Zhao G., Wu X., Tan X., Wang X., 2011. Sorption of Heavy Metal Ions from Aqueous Solutions: A Review. *Open Colloid Sci. J.* 4, 19 – 31.
- Zitzelsberger A., Schmidbauer E., 1996. Magnetic properties of synthetic milled and annealed titanomagnetite ($\text{Fe}_{2.3}\text{Ti}_{0.7}\text{O}_4$) particles 1–125 μm in diameter and analysis of their microcrystalline structure. *Geophys. Res. Lett.* 23, 2855 – 2858.